Journal of Alloys and Compounds 509 (2011) 5897–5902

Contents lists available at ScienceDirect

Journal of Alloys and Compounds

journal homepage: www.elsevier.com/locate/jallcom

Structural, optical and electrical properties of Mg-doped $CuCrO_2$ thin films by sol–gel processing

Yunfeng Wang, Yijing Gu, Tao Wang*, Wangzhou Shi

Key Laboratory of Optoelectronic Material and Device, Shanghai Normal University, 200234 Shanghai, People's Republic of China

ARTICLE INFO

Article history:
Received 14 December 2010
Received in revised form 25 February 2011
Accepted 28 February 2011

Keywords:
Sol–gel
Delafossites
$CuCrO_2$
Transparent conductive oxide

ABSTRACT

$CuCr_{1-x}Mg_xO_2$ ($x = 0, 0.03, 0.05, 0.07$) thin films were prepared on sapphire substrates by sol–gel processing. The effect of Mg concentrations on the structural, morphological, electrical and optical properties was investigated. Highly transparent ≧70% Mg-doped $CuCrO_2$ thin films with p-type conduction and semiconductor behavior were obtained. The microstructure of the systems was characterized by scanning electron microscopy and the roughness increased as the content of Mg increased. The photoluminescence spectra results indicated that it had a green luminescent emission peak at the 530 nm. In this paper, $CuCr_{0.95}Mg_{0.05}O_2$ film has the lowest resistivity of 7.34 Ω cm with direct band gap of 3.11 eV. In order to investigate the conduction mechanism, the energy band of the $CuCrO_2$ films is constructed based on the grain-boundary scattering.

1. Introduction

Thin films of transparent wide band gap n- and p-type oxide semiconductors are of much technological interest for ultraviolet (UV) optoelectronics and transparent bipolar electronics applications [1]. The visibly transparent and short wavelength absorbing p–n junction is the basic device structure in order to fabricate light emitting and solid state UV laser diodes, transparent transistors for advanced active matrix flat panel displays and in solar cells for utilizing the UV component of Sun radiation [2–4]. However, almost all of the well-known transparent conducting oxides (TCOs) such as Al-doped ZnO [5,6], Sn-doped In_2O_3 [7] and F-doped SnO_2 [8,9] are n-type semiconductor oxide, the lack of p-type TCOs severely limits the potential applications of these materials, because many of the active functions in semiconductors originate from the nature of the p–n junction.

Delafossites have gained considerable attention since the discovery of p-type conductivity in transparent $CuAlO_2$ thin films [10]. Thus far, several Cu-base delafossites have been reported such as $CuFeO_2$ [11], $CuGaO_2$ [12], $CuInO_2$ [13], $CuScO_2$ [14], $CuCrO_2$ [15–17] and Mg-doped $CuCrO_2$ and so on [18–22]. As we all known, most delafossite films were prepared by pulsed laser deposition (PLD) [23], sputtering [24], electron beam evaporation [25] and chemical vapor deposition (CVD) [26,27] and so on. There are fewer reports on the sol–gel synthesis of delafossite thin films [28–30].

In this paper, we describe the preparation and optimization of Mg-doped $CuCrO_2$ thin films by sol–gel processing. Phase-pure $CuCrO_2$ were obtained after annealing at 750 °C on sapphire substrates. We have investigated the influence of Mg content on the structural, morphological, optical and electrical properties for $CuCrO_2$ thin film.

2. Experiment

Here copper acetate monohydrate ($Cu(CH_3COO)_2 \cdot H_2O$ >98%), chromium nitrate nonahydrate ($Cr(NO_3)_3 \cdot 9H_2O$ >99%) and magnesium nitrate ($Mg(NO_3)_2 \cdot 6H_2O$ >99%) were used as precursor material and 2-methoxyethanol was used as solvent respectively. Copper acetate monohydrate and chromium nitrate nonahydrate with [Cu]/[Cr] molar ratio of 1.0 were dissolved in 2-methoxyethanol first and the concentration of solution was 0.2 M. The solution was stirred at room temperature for more than 5 h in order to get a well mixed precursor solution.

The films were deposited by spin coating route with a rotating speed of 1500 rpm for 5 s and 3000 rpm for 20 s. After each coating, the as-deposited films were dried in air at 400 °C for 5 min to evaporate the solvent and remove organic residuals. The procedures from coating to drying were repeated to achieve the desired thickness. Finally, the films were annealed at 750 °C for 1 h with a pressure of 10^{-3} Torr.

The crystal structure of the films was confirmed by conventional XRD technique with a Bruker D8 focus X'Pert diffractometer. A field emission scanning electronic microscope (FESEM) was used to determine the thickness and the surface roughness of the films by Hitachi S-4800. The photoluminescence spectrum was measured by VARIAN Cary-Eclipse 500 spectrofluorometer equipped with a 60 W Xenon lamp. The Optical transmission spectrum was investigated at 30° incidence by Aquila NKD-8000 spectrometer in the 350–1100 nm range. The dc resistivity of the film was observed with a four point probe configuration. The van-der-Pauw method was applied to measure carrier mobility and carrier density by Hall Measurement System (HMS). The Seebeck-coefficient was measured using the Physics Property Measurement System (PPMS).

* Corresponding author. Tel.: +86 21 64328884; fax: +86 21 64328894.
E-mail address: twang@shnu.edu.cn (T. Wang).

0925-8388/$ – see front matter © 2011 Elsevier B.V. All rights reserved.
doi:10.1016/j.jallcom.2011.02.175

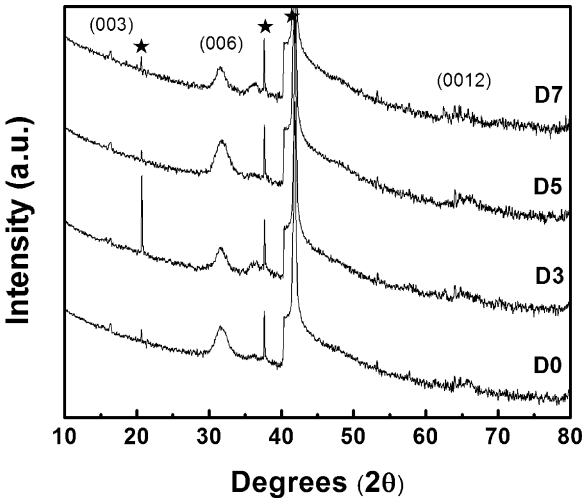

Fig. 1. XRD patterns of $CuCr_{1-x}Mg_xO_2$ ($x = 0, 0.03, 0.05, 0.07$) films on sapphire substrates annealed at 750 °C with a pressure of 10^{-3} Torr. ⋆ corresponds to the peak of sapphire substrates.

3. Results and discussion

3.1. Structural properties

In Fig. 1 the X-ray diffraction patterns of different Mg-doped $CuCrO_2$ films treated at 750 °C with a pressure of 10^{-3} Torr are given. The samples of $CuCr_{1-x}Mg_xO_2$ ($x = 0$, $x = 0.03$, $x = 0.05$, $x = 0.07$) are named as D0, D3, D5 and D7 respectively. It can be observed that the films are single 3R phase delafossite structure. The intensity of (0 0 6) peaks do not have evident change, but the Full Width at Half Maximum (FWHM) of diffraction peaks decreases with the increasing of Mg content (the FWHM of the sample D0–D7 are 1.308°, 1.172°, 1.008° and 0.810°, respectively), which may be due to the formation of the stresses by the difference in ion size between chromium and magnesium [31–33]. Fig. 2 shows the FESEM micrographs of the surface of all the films. The sample D0 clearly shows that some grains are decorated within the smooth matrix. The results suggest that the surface of films is relatively smooth, and the roughness increased with increasing doping concentrations. In order to estimate the thickness of the films, the cross-section FE-SEM is carried out, and the result is shown in Fig. 3. It can be seen that the interface between the film and the sapphire substrate is distinct. The film is tightly attached to the substrates with a very homogeneous thickness of ~103 nm in the measured range.

3.2. Optical properties

Fig. 4(a) and (b) shows photoluminescence emission spectra of the Mg-doped $CuCr_{1-x}Mg_xO_2$ films on sapphire substrates. All the films show a green luminescent emission peak at the 530 nm and blue luminescent emission peaks at the 485 nm, 445 nm, 435 nm and 424 nm. The excitation wavelength is 237 nm corresponding to 5.23 eV energy and the luminescence emission peaks occur at 2.92 eV, 2.85 eV, 2.78 eV, 2.56 eV and 2.34 eV energies, respectively. The band edge emissions can be ascribed to the $3d^9 4s^1$ and $3d^{10}$ intraband transitions involving Cu^+ ions as also reported earlier in the $CuYO_2$ [34] and $CuLaO_2$ [35] delafossite oxide insulators. The intensity of the peak at 485 nm increased and the FWHM decreased as Mg content increased. Compared to $CuLaO_2$ insulating oxide, $CuCr_{1-x}Mg_xO_2$ semiconducting oxide luminescence peaks show shift lower in the energy position, which could be ascribed to the effect of Cr on the Cu–O interaction [36]. Compared to the La ion in $CuLaO_2$, Cr ion in $CuCrO_2$ exerts stronger effect on Cu–O–Cr–O–Cu linkage due to a more favorable mixing of the 3*d* state on Cr ion affecting the Cu–O bond distance and Cu–Cu interaction.

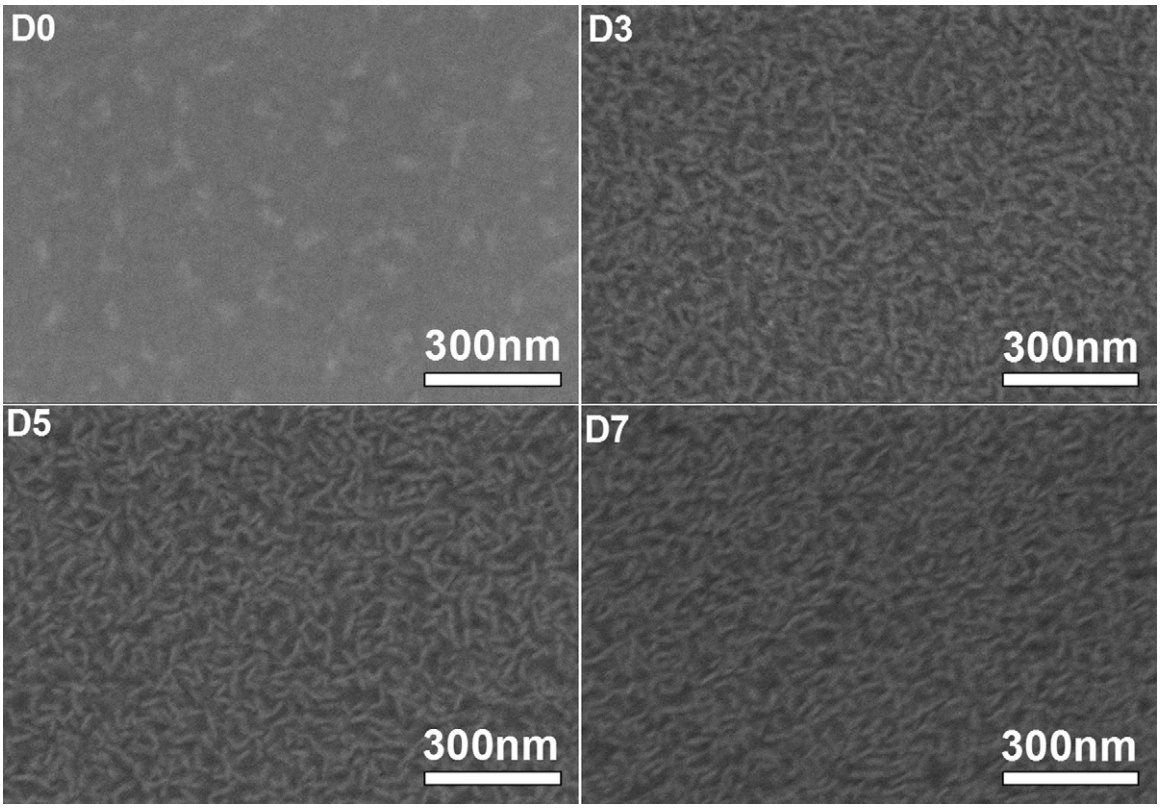

Fig. 2. FESEM micrographs of the surface of $CuCr_{1-x}Mg_xO_2$ ($x = 0, 0.03, 0.05, 0.07$) films.

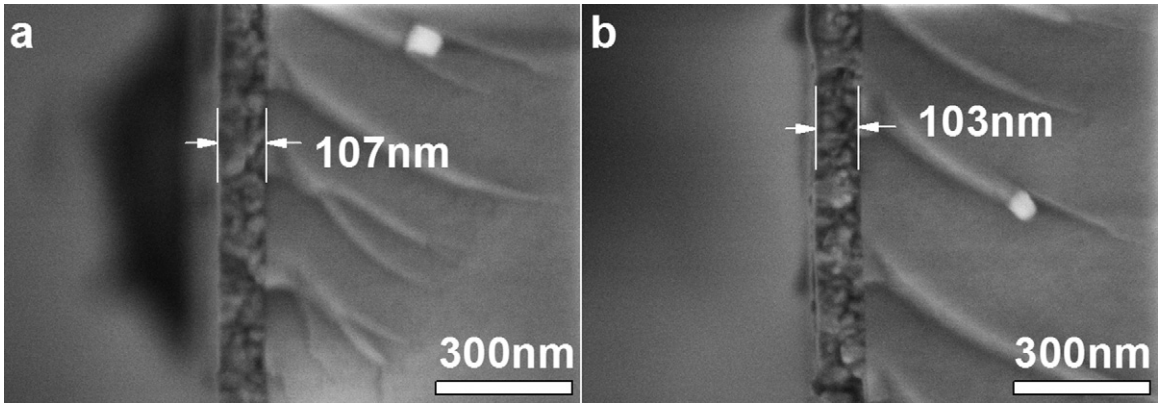

Fig. 3. FESEM micrographs of the cross section of $CuCrO_2$ (a) and Mg-doped $CuCrO_2$ (b) films.

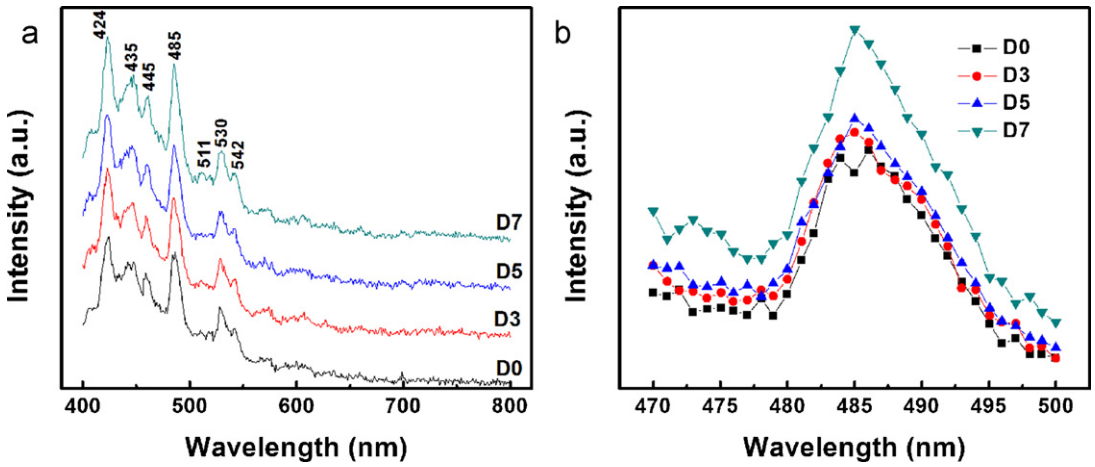

Fig. 4. Photoluminescence spectra of $CuCr_{1-x}Mg_xO_2$ (x = 0, 0.03, 0.05, 0.07) films.

The optical transmission spectra of $CuCr_{1-x}Mg_xO_2$ (x = 0, 0.03, 0.05, 0.07) films are investigated within the wavelength of 350–1100 nm, and the results are shown in Fig. 5. The transmission in the visible region decreases and the absorption edge shifts to the low wavelength as the Mg concentration increases. The average optical transmittances in the visible region are about 75%, 68%, 66% and 65% for the sample D0–D7, respectively. The low transmittance of the films can be attributed to increased photon scattering by grain boundaries. From Fig. 5, the insert shows optical absorption spectra. The absorption coefficients α can be calculated with the following formula [37]:

$$I = I_{0e}^{-\alpha t},$$

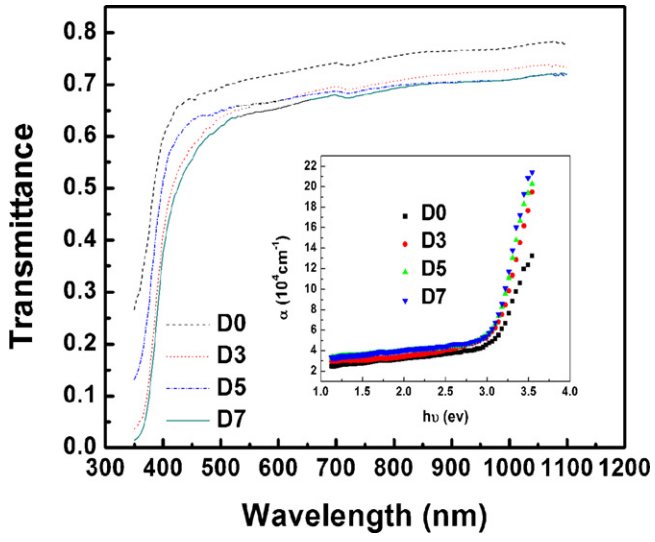

Fig. 5. Optical transmission spectra of $CuCr_{1-x}Mg_xO_2$ (x = 0, 0.03, 0.05, 0.07) films. The inset shows optical absorption spectra.

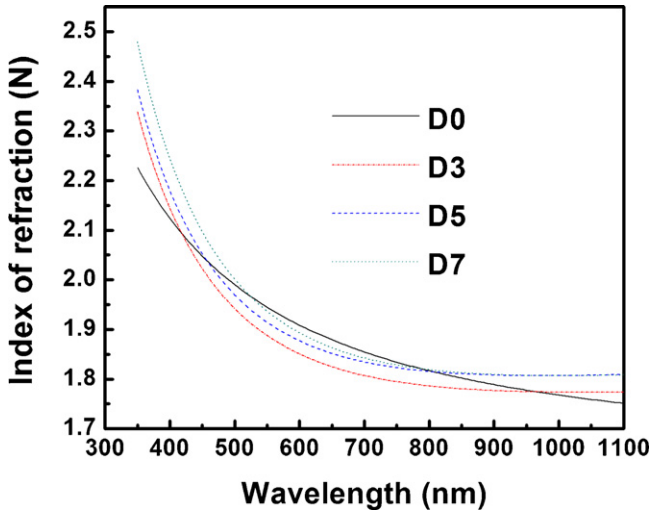

Fig. 6. Index of refraction (N) versus wavelength curves.

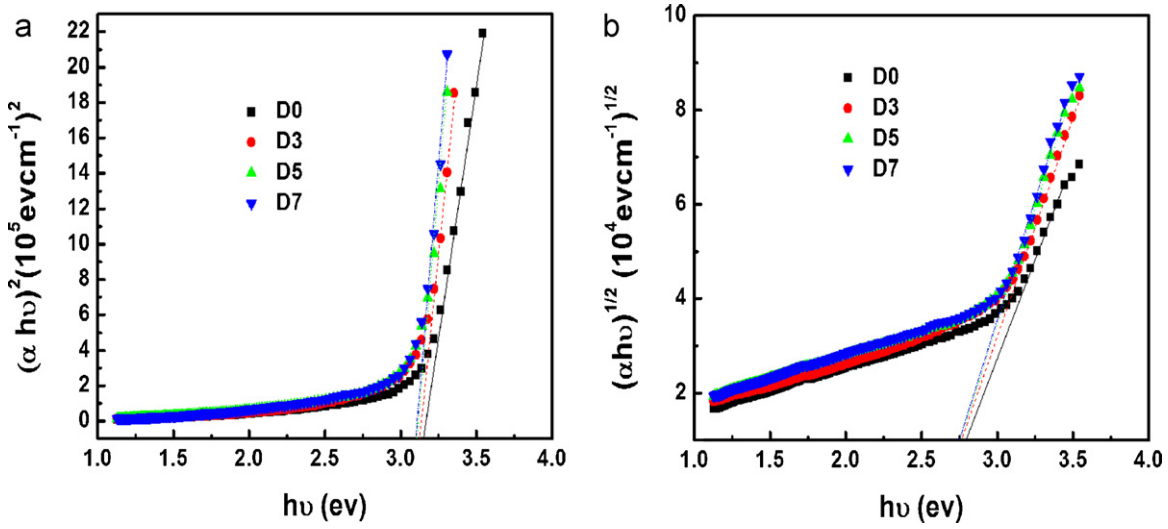

Fig. 7. Plots to test for direct allowed transition (a) and indirect band gap (b) for $CuCr_{1-x}Mg_xO_2$ films.

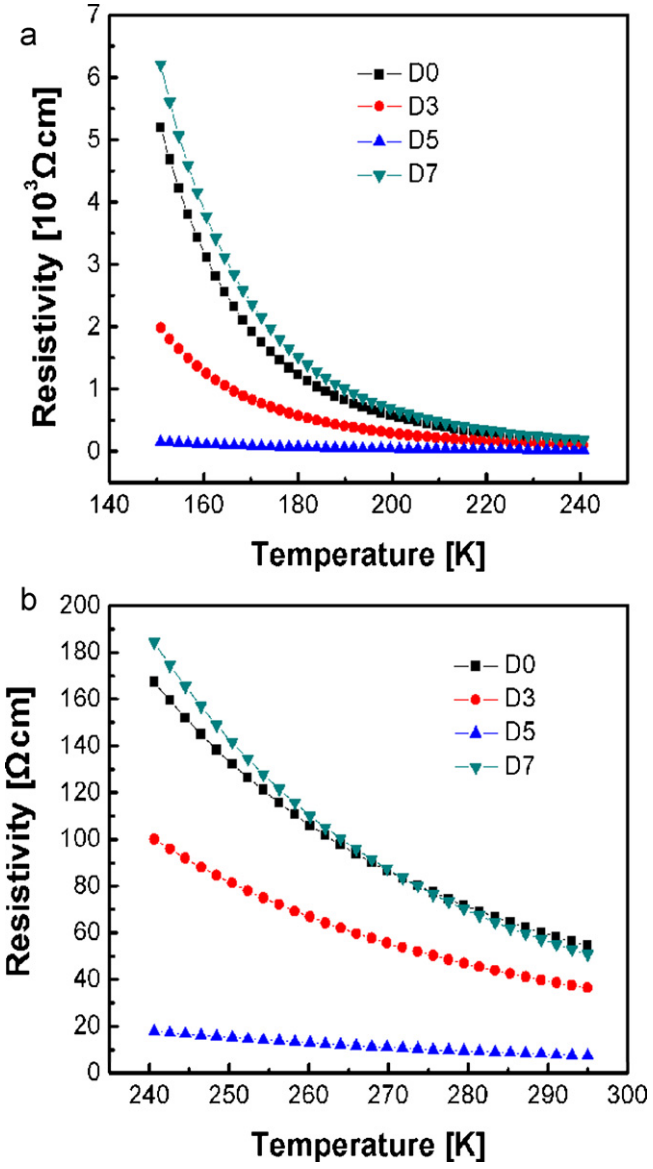

Fig. 8. The resistivity of $CuCr_{1-x}Mg_xO_2$ ($x = 0, 0.03, 0.05, 0.07$), (a) and (b) shows the results of resistivity (ρ) versus temperature (T) within the range of 150–240 K and 240–300 K respectively.

where I_0 is the incident intensity, I is the intensity of the transmitted light and t is the thickness of films. As shown in Fig. 6, for the index of refraction (N), it can be observed that N almost not any influence as introduction of Mg element in high wavelength. But the N of Mg-doped sample exhibits lower than that of $CuCrO_2$ in visible region. The index of refraction of sample D0, D3, D5 and D7 at 550 nm is 1.94, 1.89, 1.91 and 1.94 respectively.

Fig. 7 shows the direct (a) and indirect (b) band gap of sample D0–D7. The fundamental of absorption, which corresponds to electron excitation from the valance band to the conduction band, can be used to determine the nature and value of the optical band gap of the sample D0–D7. The relationship between the absorption coefficients α and the incident photon energy $h\nu$ can be fitted as [30]

$$(\alpha h\nu)^n = A(h\nu - E_g),$$

where A is a constant, E_g is the band gap of the films, $h\nu$ is the photon energy, α is the absorption coefficient. For a direct allowed transition, n is 2. For an indirect allowed transition, n is 1/2. As shown in Fig. 7(a), for the direct allowed transition, from the portion of the plot to the $h\nu$-axis it can be obtained that the optical band gaps of the samples D0–D7 are 3.15 eV, 3.12 eV, 3.11 eV and 3.10 eV, respectively. As shown in Fig. 7(b), for the indirect allowed transition, from the portion of plot to the $h\nu$-axis it can be obtained that the optical band gap of the sample D0–D7 is 2.80 eV, 2.77 eV, 2.76 eV and 2.75 eV, respectively.

3.3. Electrical properties

Fig. 8(a) and (b) shows the temperature (T) variation of resistivity (ρ) of the sampler D0–D7 within the temperature range 150–240 K and 240–300 K, respectively. It can be seen that all the films behave like semiconductors. As shown in Table 1, all the samples were verified p-conductivity by their positive See-

Table 1
Electrical properties of the sample D0–D7.

	Resistivity (Ω cm)	Thickness (nm)	Seebeck-coefficient (μV/K)	Carrier mobility ($cm^2/(V s)$)	Carrier concentration (cm^{-3})
DO	54.41	103	266	6.75	3.14×10^{15}
D3	36.41	107	202	3.47	2.53×10^{16}
D5	7.34	113	180	2.13	3.14×10^{18}
D7	50.77	105	248	6.12	6.23×10^{15}

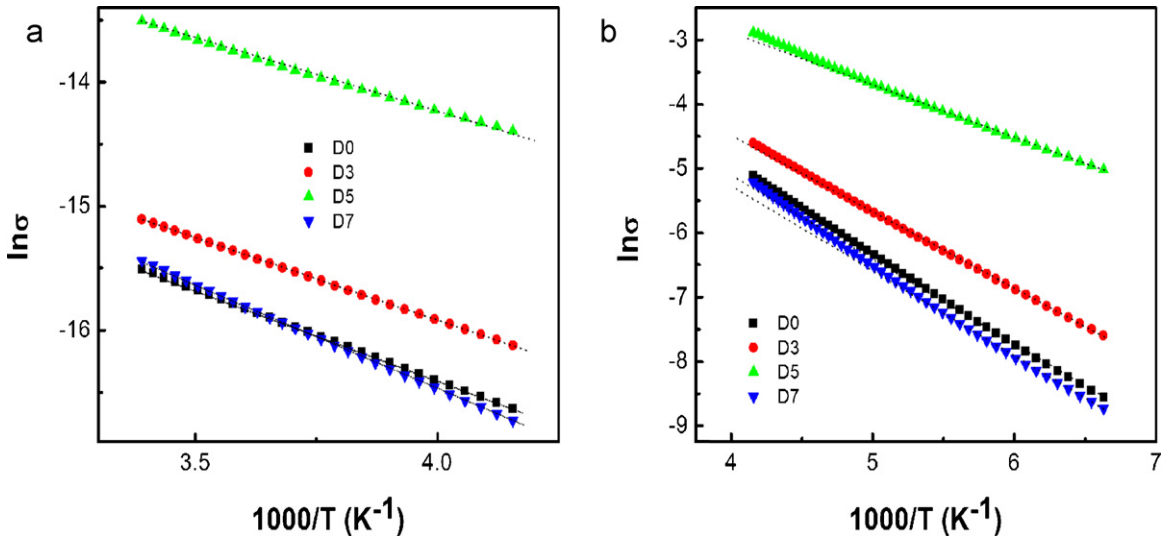

Fig. 9. (a) $\ln\sigma$ versus $1000/T$ plots of $CuCr_{1-x}Mg_xO_2$ ($x = 0$, 0.03, 0.05 and 0.07) films at 240–300 K range. (b) $\ln\sigma$ versus $1000/T$ plots at 100–240 K range.

beck coefficients [29], and the resistivity of sample D0–D7 is 54.41 Ω cm, 36.41 Ω cm, 7.34 Ω cm and 50.77 Ω cm at room temperature, respectively. The resistivity and carrier mobility of $CuCr_{1-x}Mg_xO_2$ ($x = 0$, $x = 0.03$, $x = 0.05$) films decrease with increasing Mg content. It also can be found that carrier concentration increases as increasing Mg content. However, the resistivity of sample D7 is higher than that of the sample D3 and D5, which could be due to the onset of compensating donor defects [21].

Fig. 9(a) and (b) shows $\ln\sigma$ versus $1/T$ at different temperature range. Conduction mechanism mainly is controlled by grain-boundary properties rather than others in polycrystalline films. These grain-boundaries major include high density interface state, which could capture free carrier in the crystalline and the carrier would make other carrier scattering. The high interface state also could produce space charge area on the grain boundary, so the energy band bended and the barrier Φ_b formed [38]. The conductivity of sample D0–D7 at low temperature can be modeled using grain-boundary scattering mechanism, as expressed by,

$$\sigma = A \exp\left(\frac{-e\Phi_b}{kT}\right).$$

where Φ_b is grain-boundary barrier, k is Boltzmann constant and A is a constant. Grain-boundary scattering is dominant in polycrystalline films, but all the sample show a thermal activities behavior at high temperature. So σ can be well proportional to $\exp(-E_a/kT)$ at high temperature [39,40]. Where k is Boltzmann constant, E_a is the thermal activation energy. For the 240–300 K range, grain-boundary scattering and the thermal activation behavior coexist in the films. The energy $E = E_a + \Phi_b$ value of sample D0–D7 are 301 meV, 275 meV, 180 meV and 306 meV, respectively. The change of E should be due to the differences of Fermi level of $CuCr_{1-x}Mg_xO_2$ films. The doping of Mg makes the Fermi level near the top of valence band. Carriers can be excited to the Fermi level from valence band [33,39]. For the 150–240 K range, grain-boundary scattering is dominant and the Φ_b value of sample D0–D7 are 54 meV, 45 meV, 19 meV and 57 meV, respectively.

4. Conclusion

The wide-band-gap oxide semiconductor thin films with delafossite structure were prepared by sol–gel processing. In this study, the influence of Mg content on structural, morphology, electrical and optical characteristics have been investigated. Photoluminescence emission peaks were observed at 424 nm, 435 nm, 445 nm, 485 nm and 530 nm, respectively. The result was interpreted in terms of $3d^9 4s^1$ and $3d^{10}$ Cu^+ intraband transitions. It was observed that the films behave the characteristics of microcrystalline morphology with direct band gap of 3.15 eV, 3.12 eV, 3.11 eV and 3.10 eV, respectively. The results suggested that $CuCr_{0.95}Mg_{0.05}O_2$ films can be considered as one of the candidates for TCOs with the lowest resistivity of 7.34 Ω cm. Further studies will have to systematically investigate the relationship between film structure and optoelectronic properties, which is significant to prepare p–n junctions.

Acknowledgments

Financial support is the Dr. Research Fund of Shanghai Normal University, Science and Technology Commission of Shanghai Municipality (Grant Nos. 10ZR1422300 and 09520501000), Condensed Physics of Shanghai Normal University (Grant No. DZL712)

References

[1] G. Thomas, Nature 398 (1997) 907.
[2] H. Ohta, K. Kawamura, M. Orita, M. Hirano, Appl. Phys. Lett. 77 (2000) 475.
[3] T. Kamiya, H. Hosono, Int. J. Appl. Ceram. Technol. 2 (2005) 285.
[4] K. Nomura, H. Ohta Kazushiga, T. Kamiya, M. Hirano, H. Hosono, Science 300 (2003) 1269.
[5] M. Lorenz, E.M. Kaidashev, H. von Wenckstern, V. Riede, C. Bundesmann, D. Spemann, G. Benndorf, H. Hochmuth, A. Rahm, H.-C. Semmelhack, M. Grundmann, Solid-State Electron. 47 (2003) 2205.
[6] K. Ellmer, J. Phys. D: Appl. Phys. 34 (2001) 3097.
[7] C.G. Granqvist, A. Hultaker, Thin Solid Films 411 (2002) 1.
[8] P.I. Rovira, R.W. Collins, J. Appl. Phys. 85 (1999) 2015.
[9] T. Ikeda, K. Sato, Y. Hayashi, Y. Wakayama, K. Adachi, H. Nishimura, Sol. Energy Mater. Solar Cells 34 (1994) 1.
[10] H. Kawazoe, M. Yasukawa, H. Hyodo, M. Kurita, H. Yanagi, H. Hosino, Nature 389 (1997) 939.
[11] F.A. Benko, F.P. Koffyberg, J. Phys. Chem. Solids 48 (1987) 431.
[12] K. Ueda, T. Hase, H. Yanagi, H. Kawazoe, H. Hosono, H. Ohta, M. Orita, M. Hirano, J. Appl. Phys. 89 (2001) 1790.
[13] H. Yanagi, T. Hase, S. Ibuki, K. Ueda, H. Hosono, Appl. Phys. Lett. 78 (2001) 1583.
[14] Y. Kakehi, K. Satoh, T. Yotsuya, K. Masuko, T. Yoshimura, A. Ashida, N. Fujimura, J. Cryst. Growth 311 (2009) 1117.
[15] Z. Deng, X. Fang, D. Li, S. Zhou, R. Tao, W. Dong, T. Wang, G. Meng, X. Zhu, J. Alloys Compd. 484 (2009) 619.
[16] A. Maignan, C. Martin, R. Frésard, V. Eyert, E. Guilmeau, S. Hébert, M. poienar, D. Pelloquin, Solid State Commun. 149 (2009) 962.
[17] W.T. Lim, P.W. Sadik, D.P. Norton, S.J. Pearton, F. Ren, Appl. Surf. Sci. 254 (2008) 2359.
[18] S. Götzendörfer, P. Löbmann, J. Sol-Gel Sci. Technol. 57 (2011) 157.
[19] N. Duan, A.W. Sleight, M.K. Jayaraj, J. Tate, Appl. Phys. Lett. 77 (2000) 1325.

[20] M.K. Jayaraj, A.D. Draeseke, J. Tate, A.W. Sleight, Thin Solid Films 397 (2001) 244.
[21] P.W. Sadik, M. Ivill, V. Craciun, D.P. Norton, Thin Solid Films 517 (2009) 3211.
[22] R. Nagarajan, A.D. Draeseke, A.W. Sleight, J. Tate, J. Appl. Phys. 89 (2001) 8022.
[23] H. Yanagi, S. Inoue, K. Ueda, H. Kawazoe, H. Hosono, N. Hamada, J. Appl. Phys. 88 (2000) 4159.
[24] N. Tsuboi, T. Moriya, S. Kobayashi, H. Shimizu, K. Kato, F. Kaneko, Jpn. J. Appl. Phys. 47 (2008) 592.
[25] D.S. Kim, S.J. Park, E.K. Jeong, H.K. Lee, S.Y. Choi, Thin Solid Films 515 (2007) 5103.
[26] Y. Wang, H. Gong, F. Zhu, L. Liu, L. Huang, A.C.H. Huan, Mater. Sci. Eng. B 85 (2001) 131.
[27] Y. Wang, H. Gong, Chem. Vapor Depos. 6 (2000) 285.
[28] S. Götzendörfer, C. Polenzky, S. Ulrich, P. Löbmann, Thin Solid Films 518 (2009) 1153.
[29] S. Götzendörfer, R. Bywalez, P. Löbmann, J. Sol-Gel Sci. Technol. 52 (2009) 113.
[30] G. Li, X. Zhu, H. Lei, H. Jiang, W. Song, Z. Yang, J. Dai, Y. Sun, X. Pan, S. Dai, J. Sol-Gel Sci. Technol. 53 (2010) 641.
[31] J.H. Lee, B.O. Park, Thin Solid Films 426 (2003) 94.
[32] W. Chen, J. Wang, M. Wang, Vacuum 81 (2007) 894.
[33] D. Li, X. Fang, Z. Deng, W. Dong, R. Tao, S. Zhou, J. Wang, T. Wang, Y. Zhao, X. Zhu, J. Alloys Compd. 486 (2009) 462.
[34] A. Jacob, C. Parent, P. Boutinaud, G. Le Flem, J.P. Doumerc, A. Ammar, M. Elazhan, M. Elaatmani, Solid State Commun. 103 (1997) 529.
[35] P. Boutinaud, D. Garcia, C. Parent, M. Faucher, G. Le Flem, J. Phys. Chem. Solids 56 (1995) 1147.
[36] A.C. Rastogi, S.H. Lim, S.B. Desu, J. Appl. Phys. 104 (2008) 023712.
[37] D. Li, X. Fang, Z. Deng, S. Zhou, R. Tao, W. Dong, T. Wang, Y. Zhao, G. Meng, X. Zhu, J. Phys. D: Appl. Phys. 40 (2007) 4910.
[38] X. Jiang, C. Sun, D.H. Hong, D.H. Dai, Transparent Conductive Oxide Films, High Education Press, 2008, p. 199.
[39] E.k. Liu, B.S. Zhu, J.S. Luo, Semiconductor Physics, Electronic Industry Press, Beijing, 2008, p. 413.
[40] D. Li, X. Fang, A. Zhao, Z. Deng, W. Dong, R. Tao, Vacuum 84 (2010) 851.